Ninth Canadian Conference on
Earthquake Engineering
Ottawa, Ontario, Canada
26-29 June 2007

SPATIAL RESPONSE OF INELASTIC TORSIONALLY COUPLED PRIMARY SECONDARY SYSTEMS

H.H. Mohammed[1], T.S. Aziz[2,3] and A. Ghobarah[3]

ABSTRACT

Understanding the dynamic response of nonstructural components or Secondary systems (S-systems) continues to attract substantial research attention. A large portion of project budgets is invested in S-systems compared to the main structure, referred to as the Primary system (P-system). Although most real P-systems, which support the S-systems are categorized as statically or dynamically coupled structures, research work until recently was mostly concerned with simplified elastic and inelastic response of the two degree of freedom Primary Secondary system (PS-system). Important spatial effects on the PS-system were mostly neglected. Additionally, previous research on the inelastic response of PS-systems primarily concentrated mainly on bilinear PS-systems. More likely forms of inelastic response had been mostly ignored. These inelastic response types involve spatial stiffness and strength degradation as well as spatial pinching or slip occurring in one or both subsystems. Moreover, though a wealth of numerical research on the elastic response of simplified PS-systems exists, there is little experimental work performed verifying the various techniques developed to quantify both elastic and inelastic dynamic response of PS-systems. In this paper, experimental and numerical research is presented to compare and assess inelastic spatial dynamic response of torsionally coupled PS-system. In this research work, the modified Bouc Wen Baber Noori model (BWBN model) is extended to encompass spatial pinching using the Generalized Spatial Pinching Function (GSPF). A benchmark experimental model was developed and the spatial numerical model was verified against dynamic and quazi-static experimental data. The importance of type of hysteretic inelasticity is demonstrated for torsionally inelastic PS-system response.

Introduction

Dynamic response of equipment in structures has continued to be an important subject of continuous research for the last 30 years. More recent research began addressing the practical problem involving torsionally responding elastic and inelastic PS-systems include work by (Yang and Huang 1993), (Agrawal and Datta, 1999, Agrawal 2000), (Mohammed et. al. 2003, 2004). However, substantial simplification in analyzing the behaviour of the torsionally coupled PS-system was used. Notably, no consideration was given for the type of inelasticity of the subsystems. Such effects of likely nonlinearities include stiffness degradation, strength deterioration and structural pinching or slip of one or both subsystems in a seismic event. Furthermore, the elastic S-system was typically simplified translational mass assumed to be supported at a single point. In addition, very light equipment with S-system to P-system mass ratios (m_s/m_p) ≤1% was mostly considered. Attention was also generally given to the peak response acceleration of the elastically and inelastically responding subsystems, rather than susceptibility to greater hysteretic

[1] Design Engineer at JNE Consulting Ltd., Hamilton, Ontario, Canada
[2] Principal Civil Engineer, Atomic Energy of Canada Ltd. (AECL), Mississauga, Ontario, Canada
[3] Professor at the Department of Civil Engineering, McMaster University, Hamilton, Ontario, Canada

energy dissipation in the case of inelastic response. In such a case the type of inelastic behaviour of the P-system may affect energy dissipation of the supported S-system. Pinching on the other hand is exhibited by Reinforced Concrete (RC) members with shear-dominated failure; which is characteristic of stiff RC structures. Normally however, pinching is accompanied by stiffness degradation and loss of strength for RC structural members.

Torsionally Coupled PS-System Modeling

Recently the modified BWBN model was generalized to a greater extent for bidirectional hysteresis with stiffness and strength degradation (Wang and Wen 2000). In this research the selected value of (n≥2) and (α >0) are used throughout. Hysteretic parameter equations were proposed for orthotropic supporting element under bi-directional excitation by (Wang and Wen 2000). To this formulation a practical generalization of the pinching function *h(z)* proposed by (Foliente 1995) is added herein.

$$\dot{z}_x(t) = \frac{h(z_x, z_y)}{\eta}\left\{A\dot{r}_x - \nu z_x\{|\dot{r}_x||z_x|^{n-1}(\beta+\gamma\,\mathrm{sgn}(\dot{r}_x z_x)) + \left(\frac{U_x^{\,y}}{U_y^{\,y}}\right)|\dot{r}_y||z_y|^{n-1}(\beta+\gamma\,\mathrm{sgn}(\dot{r}_y z_y))\}\right\} \quad (1)$$

$$\dot{z}_y(t) = \frac{h(z_x, z_y)}{\eta}\left\{A\left(\frac{U_x^{\,y}}{U_y^{\,y}}\right)\dot{r}_y - \nu z_y\{|\dot{r}_x||z_x|^{n-1}(\beta+\gamma\,\mathrm{sgn}(\dot{r}_x z_x)) + \left(\frac{U_x^{\,y}}{U_y^{\,y}}\right)|\dot{r}_y||z_y|^{n-1}(\beta+\gamma\,\mathrm{sgn}(\dot{r}_y z_y))\}\right\} \quad (2)$$

Where x and y are the two horizontal perpendicular directions of excitation and response components; $\dot{z}_x(t)$ is the rate of change in hysteretic parameter component $z_x(t)$ in the x-direction, $\dot{z}_y(t)$ is the rate of change in hysteretic parameter component $z_y(t)$ in the y-direction, $\dot{r}_x(t)$ is the relative velocity experienced by the structural element in the x-direction, $\dot{r}_y(t)$ is the relative velocity experienced by the structural element in the y-direction, $h(z_x,z_y)$ is the proposed generalized pinching function incorporated into the original equations presented by Wang and Wen (2000) for further generalization of the model. The energies dissipated due to bidirectional hysteretic response are therefore summed algebraically as in equation 3. Stiffness and strength degradation coefficients can be updated using equations defined by Foliente (1995), however using the total dissipated energy of equation 3.

$$\varepsilon_{hi} = \int f_{Hxi}\,dr_{xi} + \int f_{Hyi}\,dr_{yi} \quad (3)$$

Where, f_{Hxi} is the hysteretic force component due to deformation in the x direction, f_{Hyi} is the hysteretic force component due to deformation in the y direction, r_{xi} is the relative deformation of support element *(i)* in x direction, r_{yi} is the relative deformation of support element *(i)* in y direction, ε_{hi} is the total energy dissipated due to bidirectional load deformation response for support element *(i)*. The pinching function $h(z_x,z_y)$ is now also affected by the total energy dissipated due to bidirectional deformation. In equation 4 for $h(z_x,z_y)$, parameters ζ_1 and ζ_2 are updated using equations presented by Foliente (1995) respectively; however using the modified total energy equation 3. Parameters ($p, \zeta_{10}, \psi_0, \delta_\psi, \lambda$) are the same as those defined by Foliente (1995), and are assumed to be the same for the x and y direction for simplicity in this research.

$$h(z_x, z_y) = 1.0 - \zeta_1 e^{\left[\frac{-((z_x.\mathrm{sgn}(\dot{r}_x)-q_x z_u)^2+(z_y.\mathrm{sgn}(\dot{r}_y)-q_y z_u)^2)}{\zeta_2^2}\right]} \quad (4)$$

In equation 4, q_x controls the pinching level in the x-direction; q_y controls the pinching level in the y-direction. Figure 1 illustrates the three-dimensional shape of the Generalized Spatial Pinching Function (GSPF) described by the proposed generalized equation 4. The function is reminiscent of an inverted bivariate Gaussian distribution function. In figure 1 of the GSPF the parameters q_x and q_y are equated to zero and the total amount of slip or pinching is assumed to be 100 % for the purpose of demonstration. It can be inferred from the GSPF plot that the level of pinching attained for a given set of pinching model parameters is dependent also on the bidirectional loading pattern that is reflected in the values of z_x and z_y

of the structural element response. Each of the GSPF parameters is modified as a function of the dissipated energies due to deformations in the principal x and y directions.

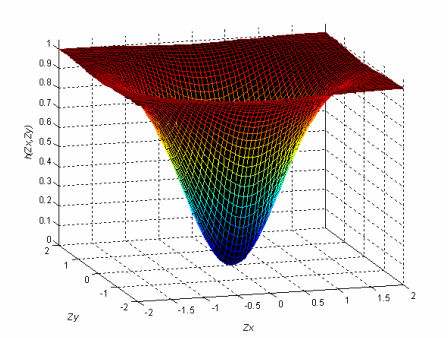

Figure 1. Generalized spatial pinching function.

State-Space Solution of the PS-system

To solve the coupled nonlinear 2nd order MDOF system equation of motion, the equation is rewritten in form of a 1st order state-space equation 5, (Barroso et. al. 1998).

$$\begin{Bmatrix} \dot{u}(t) \\ \ddot{u}(t) \\ \dot{z}(t) \end{Bmatrix} = \begin{bmatrix} 0 & I & 0 \\ -M^{-1}K_E & -M^{-1}C & -M^{-1}K_H \\ 0 & \left[\frac{dz}{du}\right] & 0 \end{bmatrix} \begin{Bmatrix} u(t) \\ \dot{u}(t) \\ z(t) \end{Bmatrix} + \begin{bmatrix} 0 \\ M^{-1} \\ 0 \end{bmatrix} F_g(t) \qquad (5)$$

Where, *I* is the identity matrix, *0* is a zero matrix, [*dz/du*] is the matrix of derivatives of the hysteretic parameter z as a function of displacement u. $F_g(t)$ is the random forcing function that could be tri-directional with two translational forces due to two perpendicular translational ground accelerations and one rotational moment due to a measured or generated ground rotational acceleration. In equation (5), static and dynamic torsional coupling capabilities were considered for both primary and secondary systems. Equation (5) is simplified to the state-equation form in equation (6).

$$\dot{q}(t) = A_{dyn}\, q(t) + F \qquad (6)$$

Where, $q(t)$ is the state vector including all variables in the 1st order ODE, A_{dyn} is the dynamical matrix including the mass, stiffness and damping matrices; *F* is the external ground acceleration vector. Equations 1, 2 and 6 for the derivative of the hysteretic parameter $z(t)$ and the state space equation of motion form a stiff set of 1st order ODEs that require for their solution a stiffly stable solution method. Either the recent Numerical Differentiation Formulas (NDFs) or the Backward Differentiation Formula (BDF) can be used to solve the 1st ODE equation 6. In this research, the more efficient NDFs option was used thought MATLAB function '**ode15s**'. The NDFs method is a variable step solution method. For a smooth presentation of results the time step for recording data should not be greater than $\Delta t = 0.01$ seconds. The P-Δ effect was considered in the solution formulation by calculating the overturning moment of each sub-system and then dividing that moment by the effective height of the supporting elements of each subsystem giving a lateral force. This force vector is multiplied by the inverse of the system mass matrix to produce a lateral acceleration that is summed with applied bidirectional ground acceleration in each time step in the appropriate direction. If and when full plastification occurs at any particular subsystem corner support, the new effective height used in the P-Δ equivalent lateral force calculation is evaluated for each corner support. Equation 7 of the plane is then used to evaluate the corresponding height at the Center of Mass (CM) of the subsystem.

$$Ax_p + By_p + Ch_{eff} + D = 0 \qquad (7)$$

Where *A, B, C* and D are the coefficients of the plane-normal.

Experimental PS-System Setup

A benchmark small-scale model of the torsioanlly coupled PS-system in figure 2 was developed to obtain experimental response data of both subsystems. One of the goals for the experimental program was the verification of the PS-system numerical model. A mass ratio of 3.2% was used in the experimental program. The shake table used was capable of delivering up to ±2 g excitation acceleration, in the frequency range of 0.0 to 20.0 Hz for a maximum pay load of 146.7 N. The maximum stroke of the shake table is ±76 mm from the centre position. Accelerometers used are capable of measuring up to ±5 g. Masses of the accelerometers attached to the two sub-systems are considered part of the overall subsystem masses. The P-system is represented by a square aluminum platform (300 mm x 300 mm), supported by circular aluminum rods of diameter 3 mm. The aluminum rods are fixed at the platform level and base level by clamp mechanisms as illustrated in 2. Steel strips fastened to the platform provide additional P-system centric mass. The P-system assembly in figure 2 can also accommodate a variety of P-system stiffness eccentricities (e) based on the number of supporting elements at each of the four corners of the P-system platform.

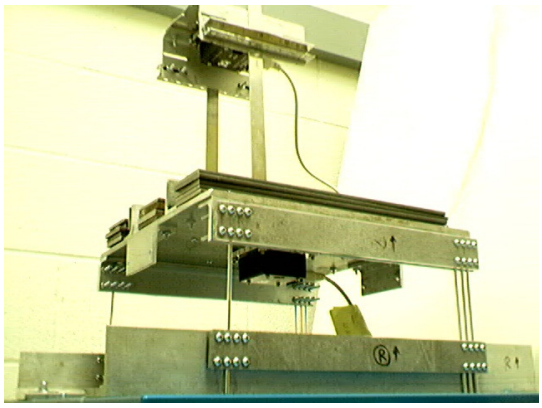

Figure 2. Experimental setup schematic.

A synthetic record was generated for the experimental analysis. The record generation process involved the use of a discretized sinusoidal function with a normally distributed random phase angle. The amplitude of the record is then based on the Kanai-Tajimi Power Spectral Density Function (PSDF) model given by equation 8.

$$G(\omega) = G_0 \frac{1+[2\xi_g(\omega/\omega_g)]^2}{[1-(\omega/\omega_g)^2]^2+[2\xi_g(\omega/\omega_g)]^2} \tag{8}$$

The parameters of this model are ground frequency ω_g, soil damping x_g and ground intensity G_o. The shear wave velocity was selected to reflect rock soil conditions (Elghadamsi et al. 1988). In this process the original duration of the generated record and the frequency content were maintained. The amplitude envelope had a parabolic rise, a constant central region at the peak value and an exponential decay. For this study the peak excitation window was set to be 30% of the total record duration of 27.8 seconds. The peak excitation level is set at 0.94 g. The generated record required no scaling.

Dynamic System Identification

After filtering the experimental response data, it was further checked in the frequency domain to ensure that the filtration process did not distort the measured amplifications. For the System Identification (SI) problem at hand there were generally 13 parameters to be identified for each subsystem under the assumption that responses in both the x and y directions for a specific structural member could be simulated with the same set of 13 hysteresis parameters. This is the case even if the force-deformation relationship for the structural member was orthotropic since this is taken care of by the yield ratio criteria

and equivalent envelope (Wang and Wen, 2000). In this research the measured responses from both subsystems are used concurrently in the SI process utilizing the full MDOF torsional PS-system numerical model. The entire lengths of experimental response records were used here for the identification process. To further enhance the convergence of the problem for both subsystem responses; weighted cost function in equation 10 was used with proportioned weights assigned for each subsystem response error. Cost function or objective function in equation 9 is then minimized for each data point.

$$F_{cost} = w_1 \sum_{i=1}^{N} (\ddot{u}^{(p)}_{experimental} - \ddot{u}^{(p)}_{model})^2 + w_2 \sum_{i=1}^{N} (\ddot{u}^{(s)}_{experimental} - \ddot{u}^{(s)}_{model})^2 + w_3 \sum_{i=1}^{N} (\varepsilon^{(p)}_{experimental} - \varepsilon^{(p)}_{model})^2 + w_4 \sum_{i=1}^{N} (\varepsilon^{(s)}_{experimental} - \varepsilon^{(s)}_{model})^2 \quad (9)$$

Where, F_{cost} is the cost function, w_i is the weight coefficient, $\ddot{u}^{(p)}_{experimental}$ is the P-system experimental response acceleration, $\ddot{u}^{(s)}_{experimental}$ is the S-system experimental response acceleration, $\ddot{u}^{(p)}_{model}$ is the P-system model response acceleration, $\ddot{u}^{(s)}_{model}$ is the S-system model response acceleration, $\varepsilon^{(p)}_{experimental}$ is the P-system calculated dissipated energy from experimental response, $\varepsilon^{(s)}_{experimental}$ is the S-system calculated dissipated energy from experimental response, $\varepsilon^{(p)}_{model}$ is the P-system calculated dissipated energy from model response, $\varepsilon^{(s)}_{model}$ is the S-system calculated dissipated energy from model response. The Levenberg-Marqaurdt approach in combination with the Numerical Differentiation Formulation (NDF) implemented in the '`ode15s`' solver, which was used to solve stiff set of differential equations for the hysteretic PS-system model proved to be a reliable combination in the SI process. Nevertheless, a sensible range of the parameter values needs to be specified to expedite the convergence.

PS-System Dynamic Response SI Results

In the following cases the measured acceleration response data and the calculated dissipated energy from the experimental measurements are compared with the numerically estimated response. The calculated dynamic response is based on the identified parameters from the modified Wang and Wen model for the MDOF PS-system small-scale model. Figures 9 and 10 show measured and estimated acceleration responses for the inelastically responding coupled P-system and coupled S-system respectively after SI 122 iterations. Although some minor discrepancies appear at some peaks, the acceleration response matching is considered to be good for both subsystems especially in the peak excitation/response window, which is the region of interest where approximately 90% of the input excitation intensity occurs for the synthetic record used.

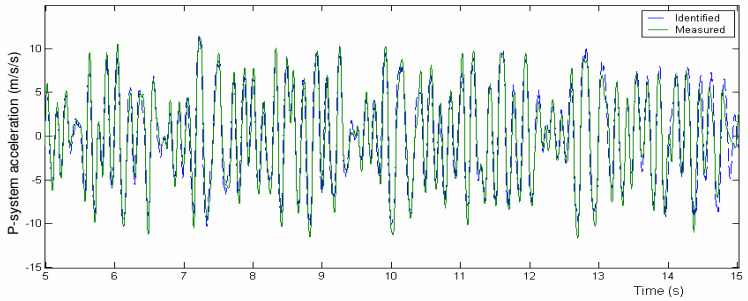

Figure 3. P-system response acceleration (m/s^2) comparison 5th to 15th second.

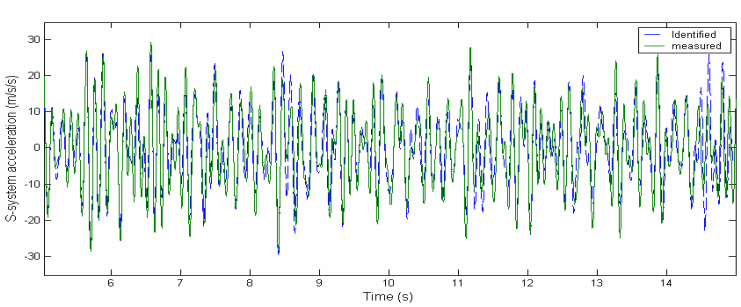

Figure 4. S-system response acceleration (m/s^2) comparison 5th to 15th second.

Model Verification for Spatial Hysteresis with Pinching

For quizi-static experimental data SI, a displacement-control approach was adopted. The output identified is the corresponding restoring force. The formulation previously presented for solving the 1st order ODE was altered and solved without the inertial and damping force components. Alternatively in the state vector q the displacement variables u_x and u_y are imposed displacement protocol. Therefore the only components of the state vector that are being solved for at each time step are the dimensionless hysteretic parameters z_x and z_y. The system of equations to be solved is given by equation (11):

$$\dot{q} = \begin{bmatrix} \dot{u}_x & \dot{u}_y & \ddot{u}_x & \ddot{u}_y & \dot{z}_x & \dot{z}_y \end{bmatrix}^T = \begin{bmatrix} q_3 & q_4 & \dot{q}_3 & \dot{q}_4 & \dot{q}_5 & \dot{q}_6 \end{bmatrix} \tag{10}$$

Where, $q = \begin{bmatrix} u_x & u_y & \dot{u}_x & \dot{u}_y & z_x & z_y \end{bmatrix}^T$ is the state vector, u_x is the imposed displacement protocol in x-direction, u_y is the imposed displacement protocol in y-direction, $\dot{u}_x$ is the imposed velocity protocol in x-direction, $\dot{u}_x$ is the imposed velocity protocol in y-direction, $\ddot{u}_x$ is the imposed acceleration protocol in x-direction, $\ddot{u}_y$ is the imposed velocity protocol in y-direction. Since quasi-static test has a long duration in reality, the identified force should therefore only represent the stiffness related resistance force as other component related to inertia and damping are physically absent. The stiffness related restoring force is obtained as:

$$\begin{Bmatrix} F_x \\ F_y \end{Bmatrix} = \begin{bmatrix} \alpha k_x & 0 \\ 0 & \alpha k_y \end{bmatrix} \begin{Bmatrix} u_x \\ u_y \end{Bmatrix} + \begin{bmatrix} (1-\alpha)k_x & 0 \\ 0 & (1-\alpha)k_y \dfrac{u_y^y}{u_x^y} \end{bmatrix} \begin{bmatrix} u_x^y & 0 \\ 0 & u_y^y \end{bmatrix} \begin{Bmatrix} z_x \\ z_y \end{Bmatrix} \tag{11}$$

Where; F_x is the identified resistance force in x-direction, F_y is the identified resistance force in y-direction, α is the Post yield stiffness to pre-yield stiffness ratio, k_x is the initial stiffness of structural element in x-direction, k_y is the initial stiffness of structural element in y-direction, u_x^y is the yield displacement in the x-direction, u_y^y is the yield displacement in the y-direction. The function for $\dot{z}_x$ and $\dot{z}_y$ include the effect of the GSPF that takes into account the pinching or slip typically observed in degrading reinforced concrete structural elements with shear dominated failure or braced steel structures that experience slip effects. In this quasi-static identification, the Levenberg-Marquardt optimization technique implemented in MATLAB as '`lsqnonlin`' was also used to determine the thirteen parameters in vector simultaneously:

$$\{P\} = \begin{Bmatrix} \alpha & n & A & \beta & \gamma & \delta_\nu & \delta_\eta & p & \zeta_{10} & \psi_0 & \delta_{\psi_o} & \lambda & q \end{Bmatrix}^T \tag{12}$$

It should be noted however that the proper specification of fixed values to some parameters might expedite convergence and error minimization.

SI of a Column with Shear Dominated Failure Under Bidirectional Deformation

The developed SI module utilizing the modified BWBN model with GSPF was used successfully in the SI of the dynamic experimental PS-system responses. However, the capabilities of the SI module were not fully tested. Experimental force-displacement responses data from work conducted by Maruyama et. al. (1984) on short Reinforced Concrete (RC) columns under bilateral load histories was used in this model verification case. Results of specimens column O-B4 where selected. Columns O-B4 was subjected to the theoretical displacement protocols shown in Figure 5b. The results of the SI process for experimental data of column O-B4 are shown in Figure 6 for the East-West (EW) and North-South (NS) directions respectively. Since both EW and NS displacement protocols pass through the origin for this short column specimen whose failure is shear dominated, hysteretic pinching is present in both the EW and NS directions. Figures 6 and 7 show that the proposed GSPF used for SI successfully detects the bidirectional hystereses with pinching. Table 1 lists the upper bounds, lower bounds and identified parameter values for specimen O-B4. Specimen O-B4 was tested without the application of any axial loading.

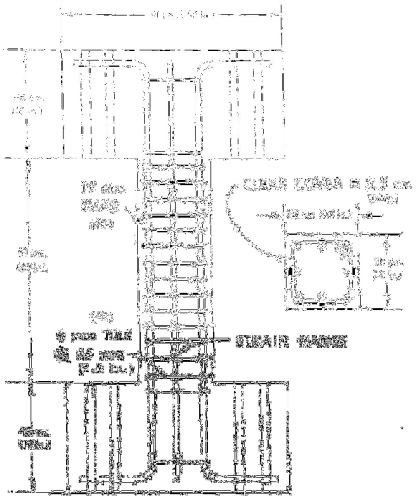

(a) Short columns O-B4 details (Maruyama et. al. 1984)

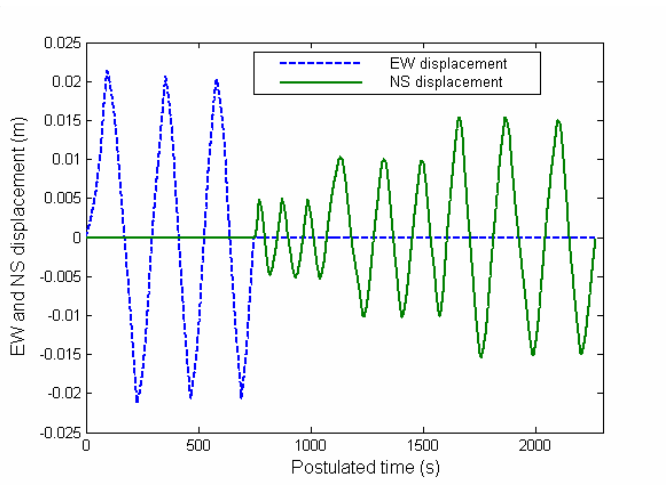

(b) Digitized displacement path

Figure 5. Details of short columns O-B4 and O-S.

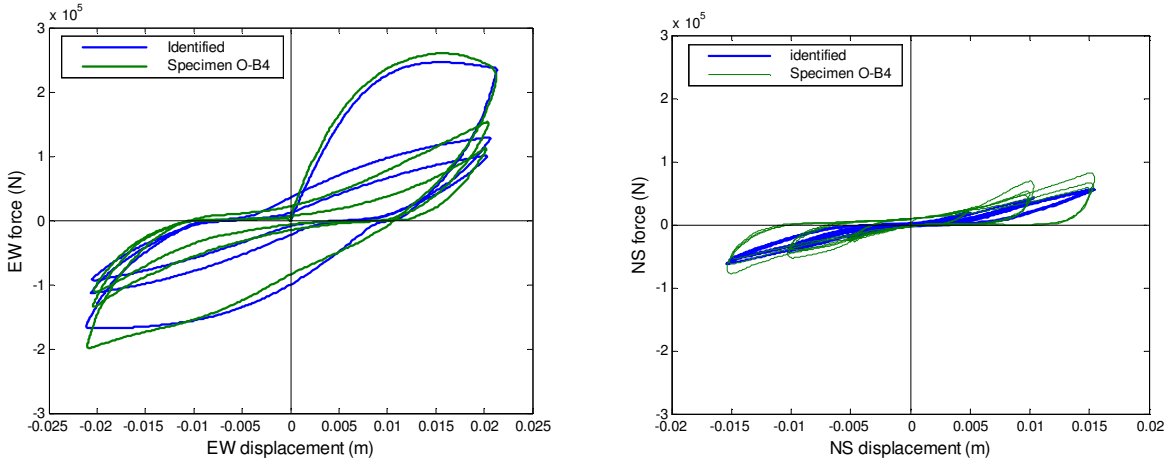

Figure 6. Column O-B4, identified & experimental hystereses in EW-direction & NS-direction.

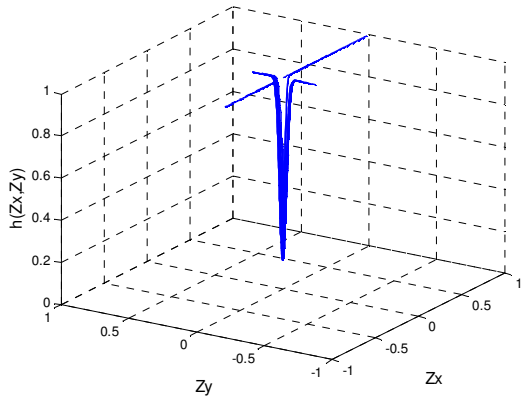

Figure 7: Identified GSPF for specimen O-B4

Table1. Parameter bounds and identified values for specimen O-B4.

Parameter No.	Parameter Symbol	Lower Bound	Upper Bound	Initial Guess	Identified Value
1	α	0.0001	0.10	0.0001	$9.4135*10^{-4}$
2	n	1.00	10.0	2.00	1.8052
3	A	1.00	1.10	1.00	1.0021
4	β	-2.50	2.50	0.95	0.8171
5	γ	-2.50	2.50	0.05	-0.4616
6	δ_ν	0.00	0.20	$2.37*10^{-6}$	$5.4601*10^{-6}$
7	δ_η	0.00	0.20	$1.05*10^{-7}$	$3.8569*10^{-6}$
8	p	0.00	4.00	$1.0*10^{-6}$	$6.1942*10^{-6}$
9	ζ_{10}	0.00	0.99	0.80	0.8642
10	ψ_0	0.00	0.90	0.04	0.0374
11	$\delta_{\psi 0}$	0.00	0.20	$2.32*10^{-7}$	$8.9024*10^{-10}$
12	λ	0.00	2.20	0.002	$8.7143*10^{-6}$
13	q_x	0.00	0.10	0.00	0.0061
14	q_y	0.00	0.10	0.00	$2.2204*10^{-14}$

Effect of the Type of Inelasticity on the PS-System Response

Several numerical torsionally coupled PS-systems models were considered having a variety of S-system location eccentricities as shown in figure 8, where the smaller dark grey square represents the S-system location. The large light grey square in figure 8 represents the P-system in plan view. A velocity amplitude; sinusoidal translational sweep was used as base excitation in the x-direction. For the inelastically responding PS-system the use of an energy-based index was deemed suitable approach in describing the damage potential for the inelastically responding PS-system. Equation 13 is the MDOF generalization for a torsionally coupled subsystem, of the energy damage index previously proposed by (Gosain et al 1977).

$$DI_E = \frac{\sum_i E_h}{\sum_i F_{yi}\delta_{yi}} \qquad (13)$$

Where DI_E is the dissipated hysteretic-energy, based damage-index. $\sum_i E_h$ is the total dissipated

hysteretic energy of all of the subsystem's structural supports. $\sum_i F_{yi}\delta_{yi}$ is the summation of unit reference dissipated energies for subsystem supports. A constant ratio $(\omega_{\theta p}/\omega_{tp}) = 1.5$ was maintained for the P-system, where $\omega_{\theta p}$ is the uncoupled P-system rotational frequency and ω_{tp} is the uncoupled P-system translational frequency. Two different P-system static coupling cases were considered. The first case being a perfectly symmetric P-system with 0.0% static coupling. The second case was P-system with 20.0% static coupling in the y-direction. A S-system with mass ratio 3.2% was used for these analyses. The S-system was considered to be perfectly symmetric at all locations of attachment. Figure 9 shows the peak dissipated energy by the S-system for the various attachment locations. In figure 9, on the horizontal axis, (1) refers to the results of the smoothed bilinearly responding; initially modally tuned PS-system, whereas (2) refers to the results of the smoothed bilinear pinching; initially modally tuned PS-system. Finally, (3) refers to the smoothed bilinear; pinching and degrading; initially modally tuned PS-system. In Figure 9a where the P-system torsionally symmetric and has initial $(\omega_{\theta p}/\omega_{tp}) = 1.5$, it is observed that when pinching is introduced into the subsystem model in the absence of P-system static coupling, the amount of hysteretic energy dissipated is slightly reduced for most of the seven location eccentricities of the S-system. For the central location 4, which coincides with the P-system CM, the reduction is significant. Introduction of degradation significantly reduces the dissipated energy in the S-system since degradation in stiffness and loss of strength can rapidly reduce the P-system's fundamental modal frequency causing detuning. Having pinching without degradation or loss of strength causes tuning and detuning to be reoccurring throughout the response of both subsystems. In Figure 9b, the introduction of 20.0% static coupling appears to keep the responses of the smoothed bilinear PS-system and the smoothed bilinear pinching PS-system very close. There is however noticeable increase in the damage index for locations 1, 2, 3, 4, 5 and 7 when the pinching is activated in the subsystem models. The activation of subsystem degradation in stiffness and loss of strength significantly reduces the S-system's damage in all locations due to fast detuning.

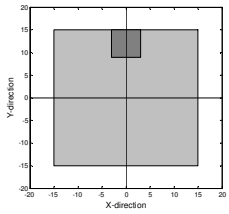

(a) Location 1

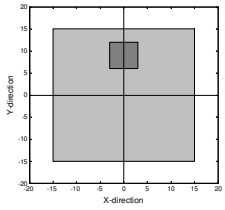

(b) Location 2

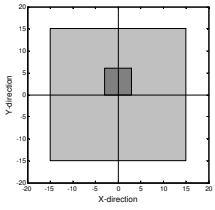

(c) Location 3

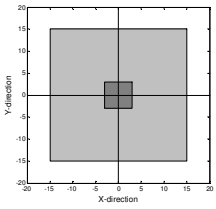

(d) Location 4

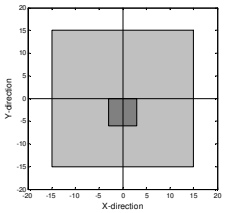

(e) Location 5

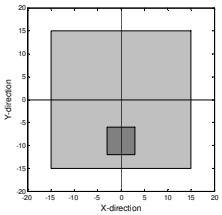

(f) Location 6

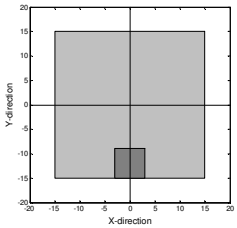

(g) Location 7

Figure 8. Unidirectional S-system location eccentricity cases 1 to 7.

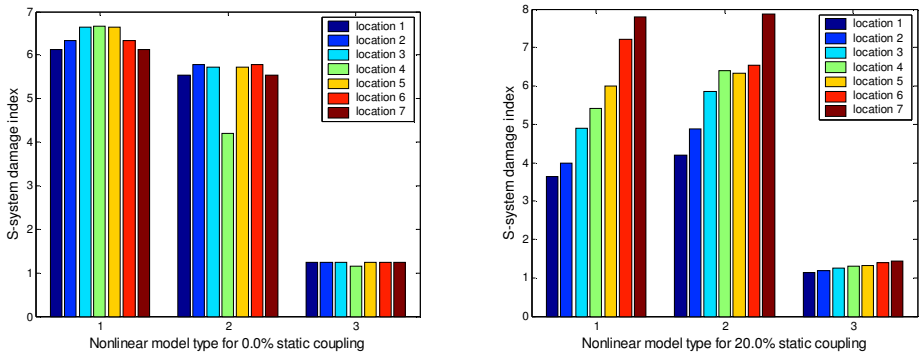

(a) (b)

Figure 9. S-system DI_E , P-system static coupling is 0.0% & 20.0% in the y direction, $\left(\omega_{\theta p}/\omega_{tp}\right)=1.5$.

Conclusions

In this research, an inelastic model using the bidirectional modified BWBN was presented for the time history analysis of torsionally coupled PS-system having both static and dynamic coupling capabilities considering P-Δ effects. A generalized bidirectional pinching function was proposed based on the unidirectional pinching model presented by Foliente (1995). The formulation was implemented in a MATLAB code that is capable of resembling any type of structural hysteretic inelasticity for either subsystem under multidirectional base excitation; with the model parameters properly identified. A force controlled (dynamic) input-output SI module was developed utilizing the Levenberg-Marquardt approach implemented in MATLAB for identifying a MDOF dynamic system exhibiting nonlinear response. Verification of the nonlinear MDOF model as well as the efficiency of the SI module; was demonstrated using the SI of the experimentally tested PS-system. The application of the SI module was adjusted for quasi-static displacement controlled experimental results. The application of the SI module was extended to the identification of structural elements exhibiting severe nonlinear behaviour including stiffness and strength degradation, as well as pinching under a bidirectional displacement protocol. Reported quasi-static experimental bidirectional force-deformation hystereses; were predicted with good accuracy by the modified BWBN with the proposed GSPF. The SI results indicate the reliability of the model and the efficiency of the SI module for parameter identification. The selected bounds for the identification process of each of the studied cases were found to be adequate. The numerical analysis considering S-system location eccentricity, P-system static coupling and PS-system type of inelasticity demonstrated that consideration of the subsystem type of inelastic hysteresis is an important factor for inelastically responding torsionally coupled PS-systems as it can dictate the damage susceptibility of the S-system where the initial elastic PS-system is the same. Of particular significance was the observation that the presence of pinching and no degradation in stiffness or strength damage susceptibility may increase for certain coupling cases as compared to smoothed bilinear response of the subsystems.

References

Agrawal, A.K. and Datta, T.K., 1999. "*Seismic Behavior of a Secondary System on a Yielding Torsionally Coupled Primary System,*" JSEE, Vol. 2, No.1, PP. 35-46, Fall.

Agrawal, A.K., 2000. "*Behavior of Equipment Mounted over a Torsionally Coupled Structure With Sliding Support*," Engineering Structures, Vol. 22, pp. 72-84.

Barroso L. R., Breneman S. E. and Smith H. A., 1998. "*Evaluating the effectiveness of actively controlled structures within the context of performance-based engineering*," Proceedings of the 6th U.S. National Conference on Earthquake Engineering, Seattle, Washington, May 31st – June 4th, paper 123.

Elgadamsi, F. E., Mohraz, B., Lee, C. T., and Moayyad, P., 1988. "*Time-Dependent Power Spectral Density of Earthquake Ground Motion*," International journal soil dynamics and earthquake engineering, No. 1, pp. 15-21.

Foliente G.C., 1995. "*Hysteretic modeling of wood joints and structural systems*," Journal of Structural Engineering, Vol. 121 (6), pp.1013-1022.

Gosain N. K., Brown R. H., Jirsa J. O., 1977. "Shear requirements for load reversals on RC members," Journal of structural engineering, ASCE, Vol. 103, No. 7, pp.1461-1476.

Maruyama K., Ramirez H, Jirsa J., 1984. "*Short RC columns under bilateral load histories*," Journal of structural engineering, Vol. 110, No. 1, pp. 120-137, January.

Mohammed H. H., Aziz T. S., Ghobarah A., 2003. "*Experimental response of non-structural components on yielding structures under seismic excitation*," Proceeding of the extreme load conference, Toronto, ON., Canada.

Mohammed H. H., Aziz T. S., Ghobarah A., 2004. "Nonlinear experimental response of primary-secondary systems under repeated seismic excitation," 13th world conference on earthquake engineering, Vancouver, BC., Canada, paper no. 3369, August 1st-6th.

Wang C. H., Wen Y. K., 2000. "*Evaluation of pre-Northridge low-rise steel buildings. I: modeling*", ASCE Journal of Structural Engineering, pp. 1160-1168.

Yang, B.Y. and Huang, W.H., 1993. "*Seismic Response of Light Equipment in Torsional Buildings*," Earthquake Engineering and Structural Dynamics, Vol. 22, pp. 113-128.